Supporting Information for

Phase Evolution of Electrochemically Potassium Intercalated Graphite

Hiroo Onuma,[a] Kei Kubota,[a,b] Shotaro Muratsubaki,[a] Wataru Ota,[c] Maxim Shishkin,[b] Hirofumi Sato,[b,c] Koichi Yamashita,[b,d] Satoshi Yasuno,[e] and Shinichi Komaba*[a,b]

[a.] *Department of Applied Chemistry, Tokyo University of Science, 1-3 Kagurazaka, Shinjuku-ku, Tokyo 162-8601, Japan.*

[b.] *Elements Strategy Initiative for Catalysts and Batteries (ESICB), Kyoto University, 1-30 Goryo-Ohara, Nishikyo-ku, Kyoto 615-8245, Japan.*

[c.] *Department of Molecular Engineering, Kyoto University, Nishikyo-ku, Kyoto 615-8510, Japan.*

[d.] *Department of Chemical System Engineering, Graduate School of Engineering, The University of Tokyo, 7-3-1 Hongo, Bunkyo-ku, Tokyo 113-8656, Japan.*

[e.] *Japan Synchrotron Radiation Research Institute (JASRI), 1-1-1 Kouto, Sayo-gun, Hyogo, 679-5198, Japan.*

**Corresponding author: komaba@rs.tus.ac.jp*

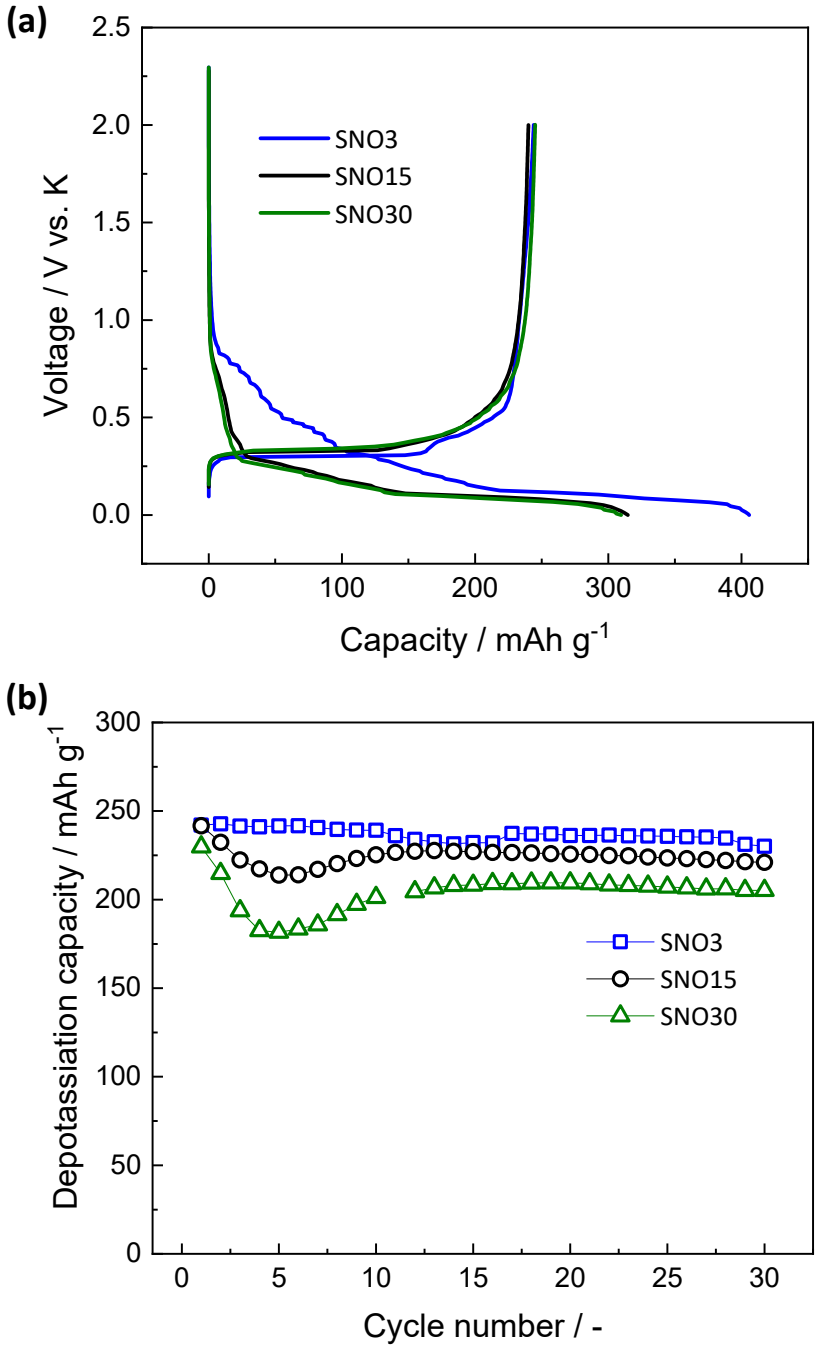

Figure S1 Particle size dependence. (a) First galvanostatic charge-discharge curves and (b) depotassiation-capacity retention of coin-type K||graphite cells tested in the voltage range of 0.0-2.0 V at 25 mA g^{-1}. Different median size of graphite particles (e.g., number in SNO3 refer to the median size of 3 µm) were used with 10 wt% PVdF binder in the electrode. Electrolyte used was 1 mol dm^{-3} KFSA/EC:DEC (= 1:1 v/v).

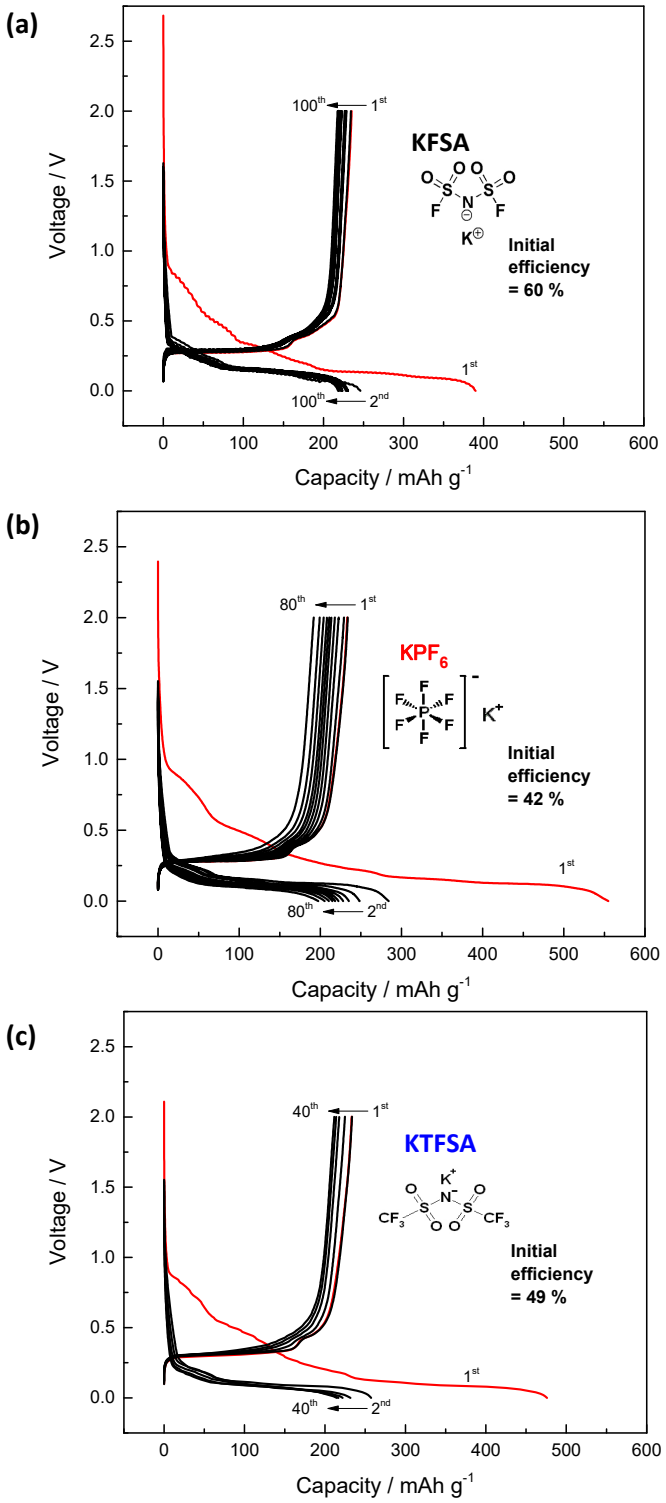

Figure S2 Electrolyte salt dependence. Galvanostatic charge-discharge curves of coin-type K||graphite cells tested in the voltage range of 0.0-2.0 V at 25 mA g^{-1}; (a) 1.0 mol dm^{-3} KFSA/EC:DEC (= 1:1 v/v), (a) 0.8 mol dm^{-3} KPF_6/EC:DEC (= 1:1 v/v), and (c) 1.0 mol dm^{-3} KTFSA/EC:DEC (= 1:1 v/v). 10 wt% PVdF was used as a binder.

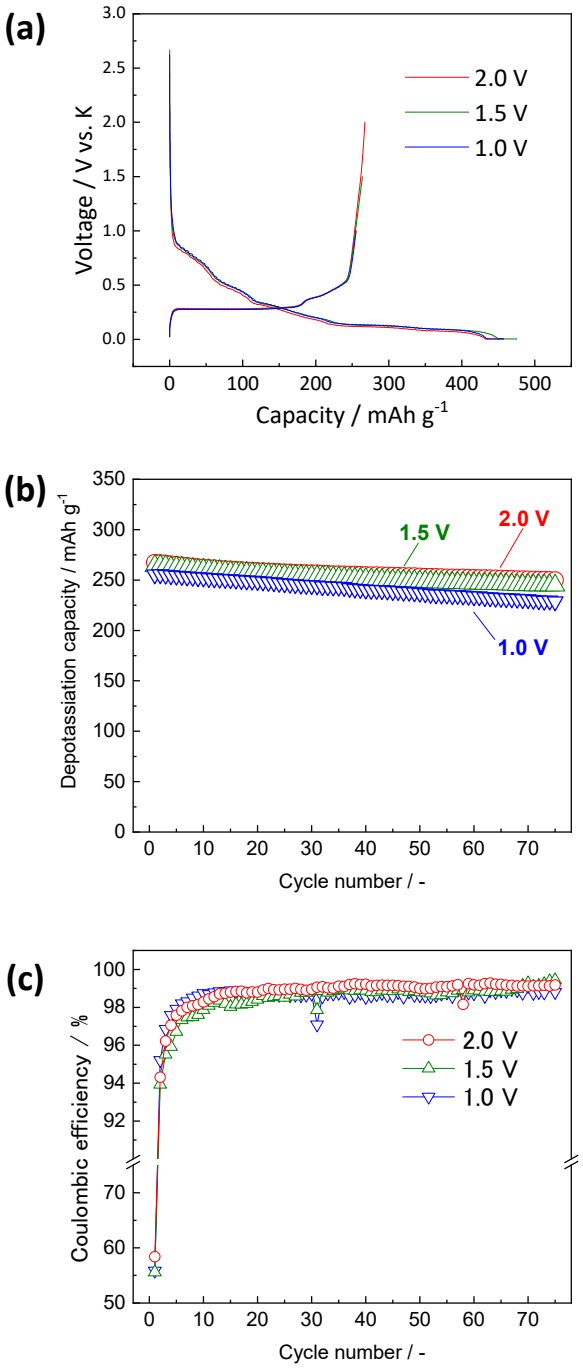

Figure S3 Upper cutoff voltage dependence. (a) Initial charge-discharge curves, (b) capacity retention, and (c) Coulombic efficiency of coin-type K||graphite cells in the voltage ranges of 0.002-1.0 V, 0.002-1.5 V, and 0.002-2.0 V in the CC-CV mode at 25 mA g^{-1} until reaching the targeted voltages and kept at 0.002 V for 5 h. 10wt% PVdF binder and 1.0 mol dm^{-3} KFSA/EC:DEC (= 1:1 v/v) electrolyte were used. The dips in Coulombic efficiency at the 31st cycle were caused by stopping and restarting the tests. One can see tiny reduction of capacity retention when the upper cutoff voltage is lower. SEI formed on the graphite particles might be modified depending on the upper cutoff voltage.

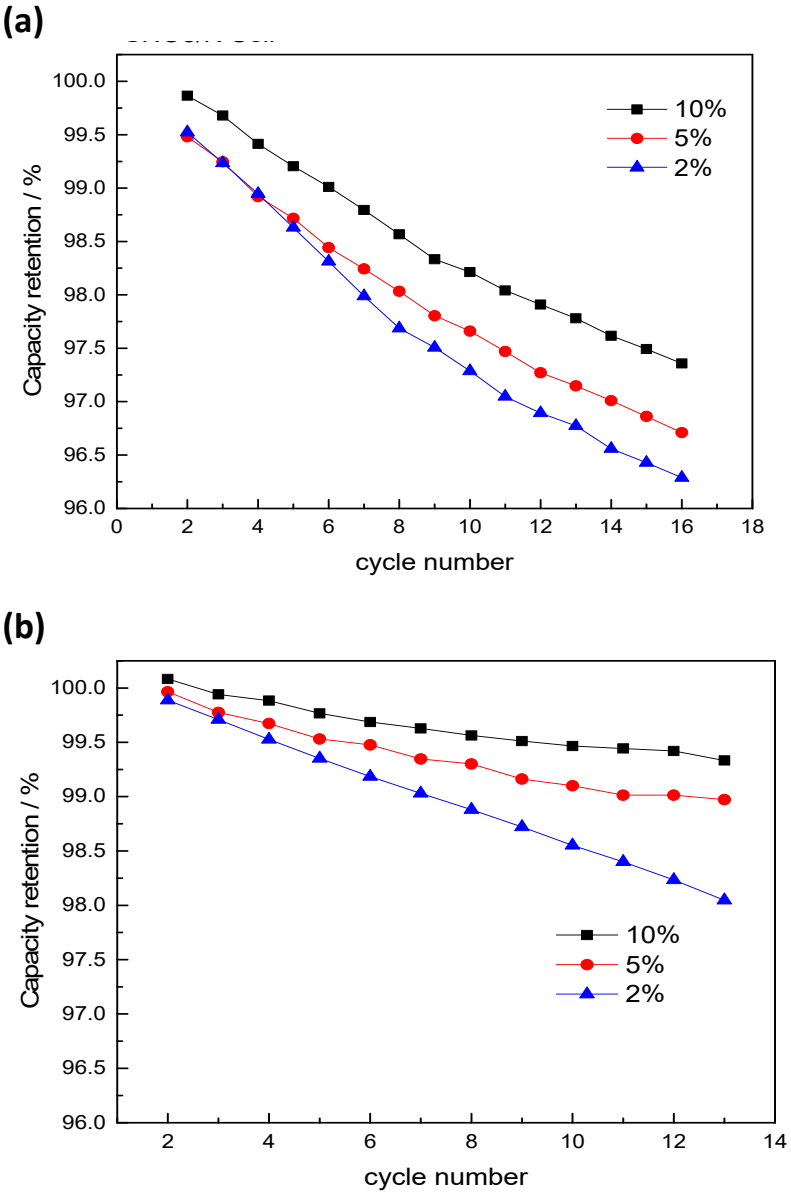

Figure S4 PVdF content dependence. Capacity retention of deintercalation capacities of coin-type (a) K||graphite and (b) Li||graphite cells in the voltage range of 0.002-2.0 V vs. AM (AM = alkali metal) in the CC-CV mode at 25 mA g^{-1} until reaching the targeted voltage and kept at 0.002 V vs. AM for 5 h. 2, 5, and 10wt% PVdF binder was used. The electrolyte solutions used in the K and Li cells were 1.0 mol dm^{-3} AMFSA/EC:DEC (= 1:1 v/v).

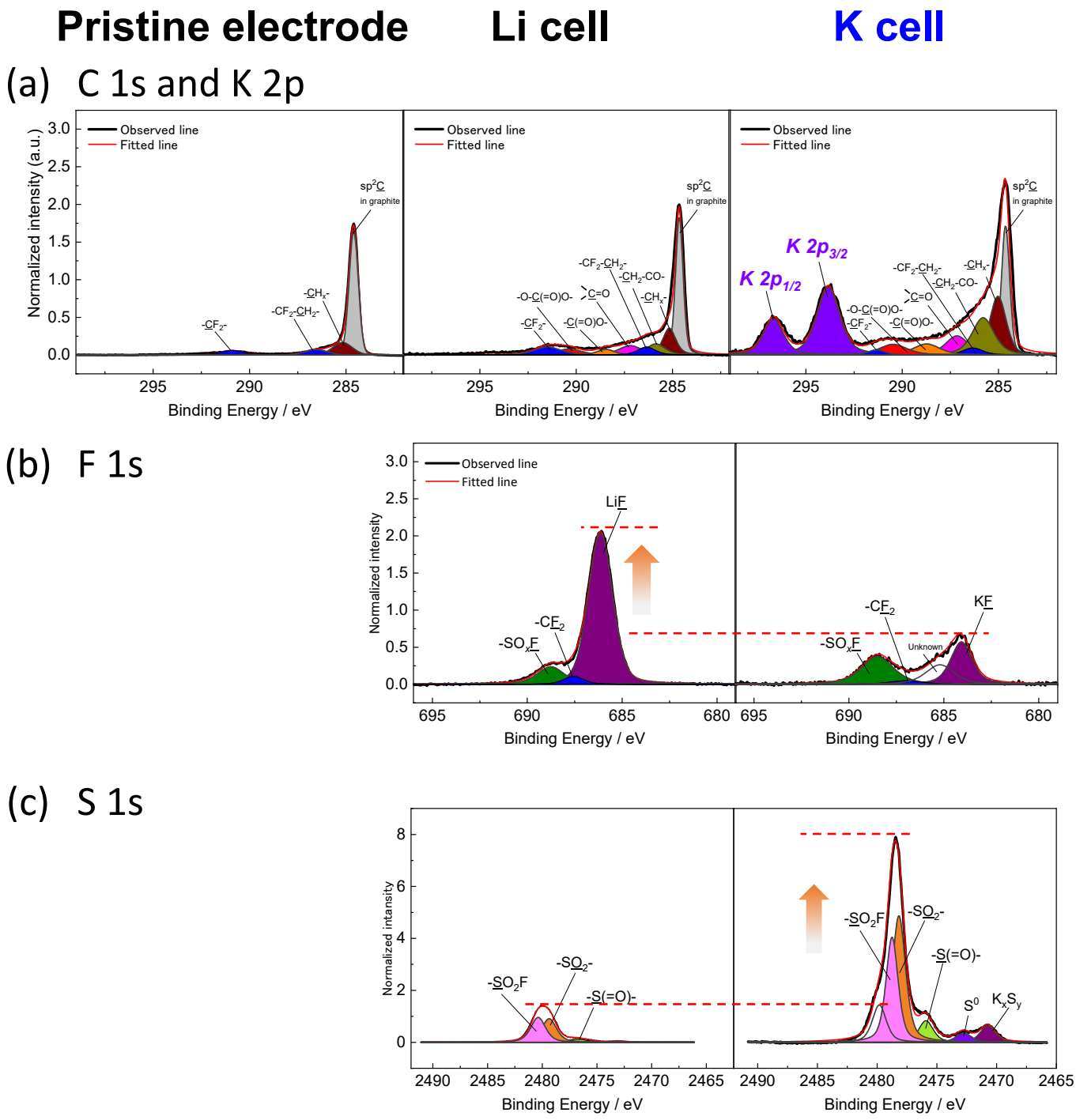

Figure S5 (a) C 1s and K 2p, (b) F 1s, and (c) S 1s HAXPES spectra of pristine and cycled graphite electrodes with 10 wt% PVdF binder in Li and K cells. 1.0 mol dm^{-3} AMFSA (AM = Li or K) /EC:DEC (= 1:1 v/v) electrolytes were used. HAXPES intensity was normalized by sp^2 C peak area.

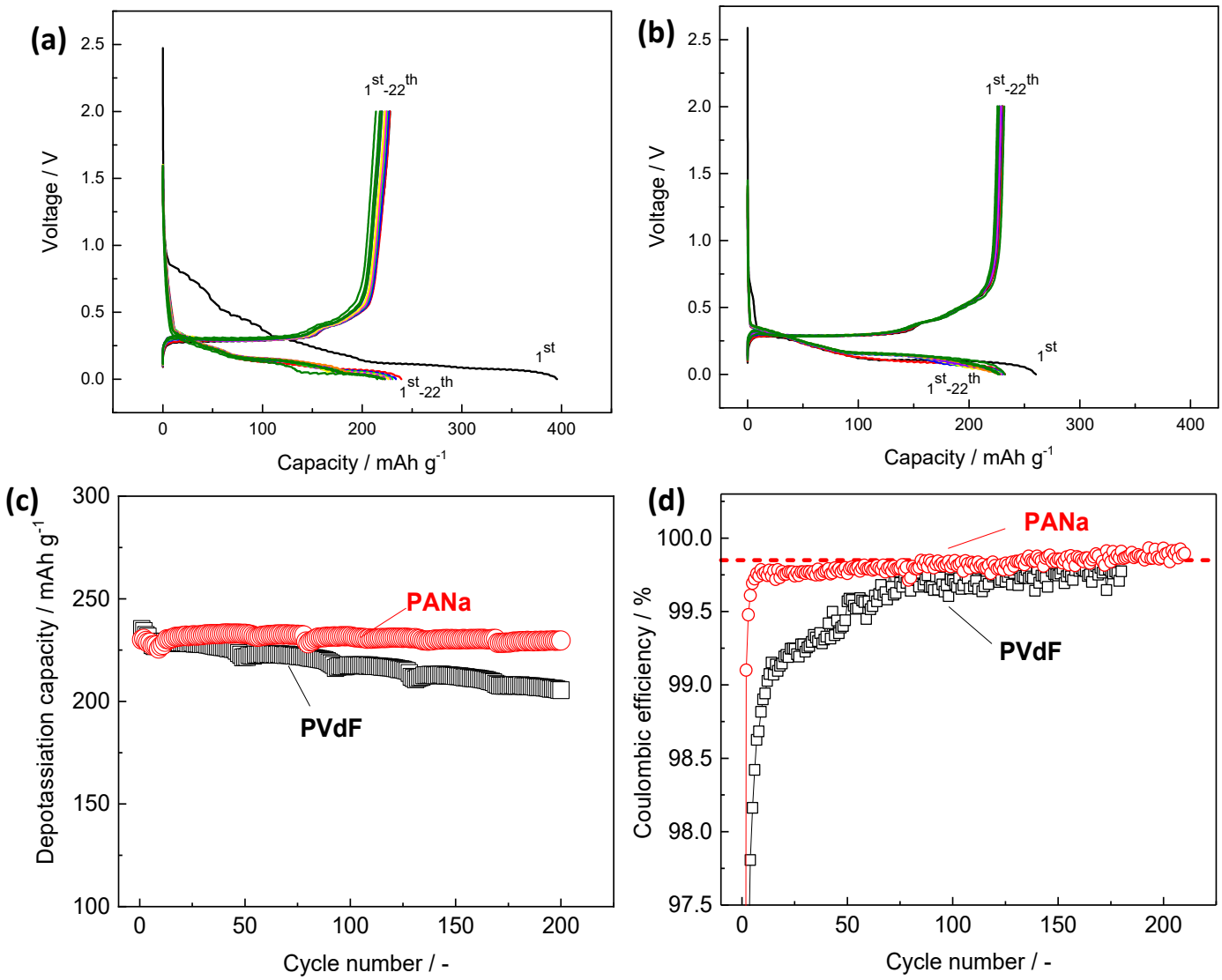

Figure S6 Binder dependence. (a, b) Galvanostatic charge-discharge curves and (c) cycle stability and (d) Coulombic efficiency of graphite electrodes with (a) 10 wt% PVdF and (b) 10 wt% PANa binder in coin-type K cells tested in the voltage range of 0.0-2.0 V in the CC mode at 25 mA g^{-1}. 1.0 mol dm^{-3} KFSA/EC:DEC (= 1:1 v/v) electrolyte was used.

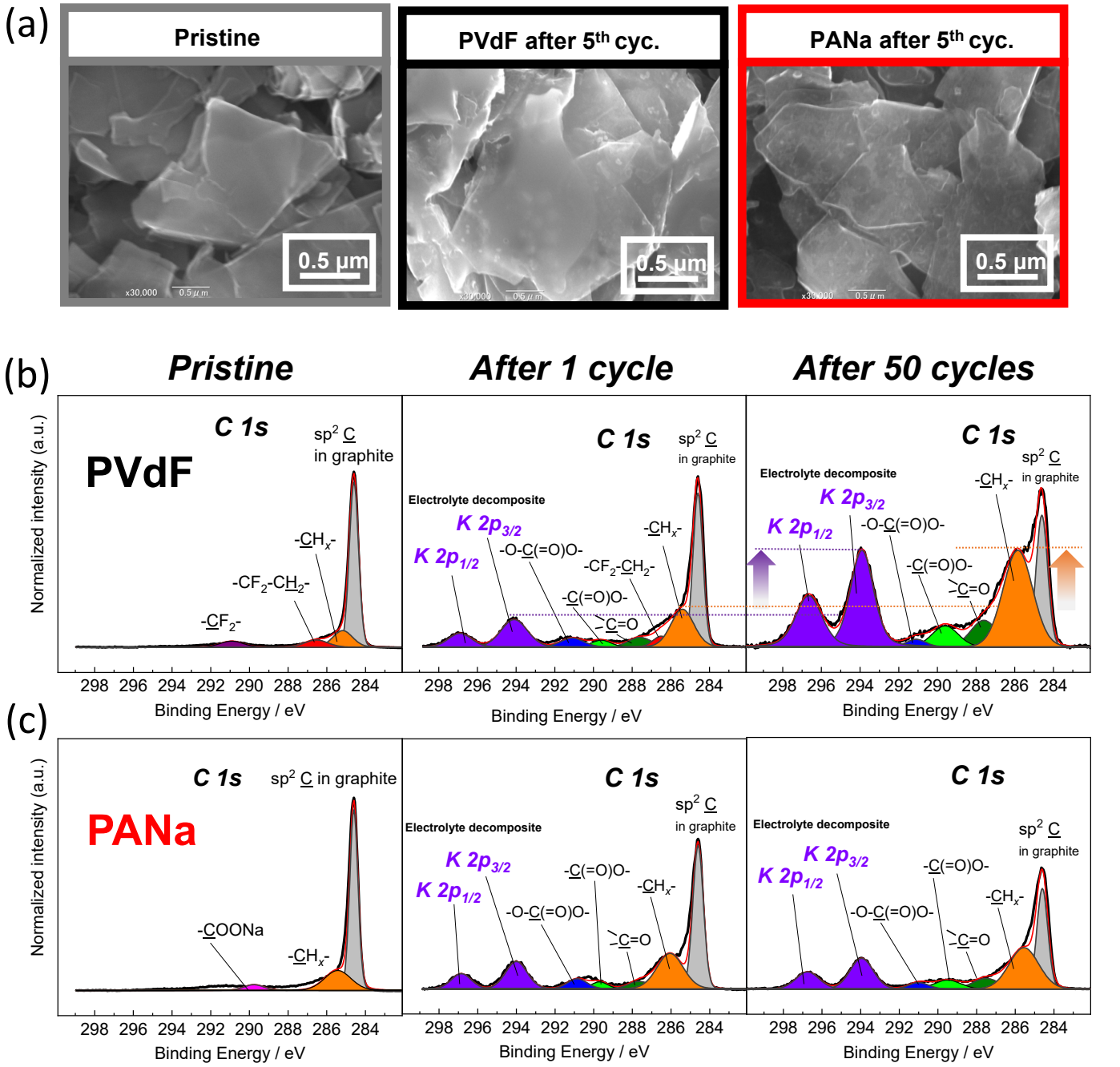

Figure S7 (a) SEM images and (b, c) HAXPES spectra of pristine and cycled electrodes with (b) 10 wt% PVdF and (c) 10 wt% PANa binder in K//graphite cells. 1.0 mol dm^{-3} KFSA/EC:DEC (= 1:1 v/v) electrolytes were used. HAXPES intensity was normalized by sp^2 C peak area.

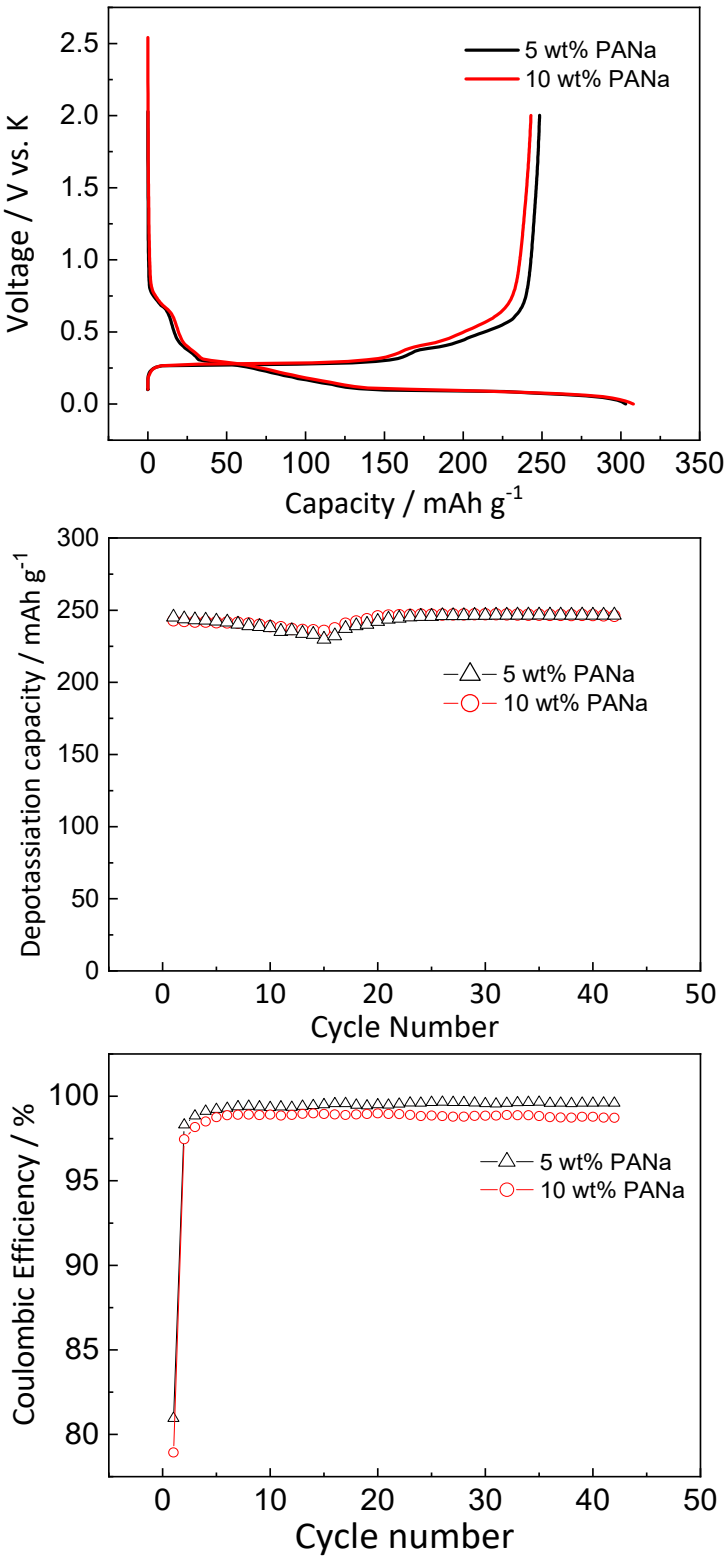

Figure S8 Binder amount dependence. (a) Galvanostatic charge-discharge curves, (b) cycle stability, and (c) Coulombic efficiency of graphite electrodes with 5 or 10 wt% PANa binder in coin-type K cells tested in the voltage range of 0.0-2.0 V in the CC mode at 25 mA g^{-1}. 1.0 mol dm^{-3} KFSA/EC:DEC (= 1:1 v/v) electrolytes was used.

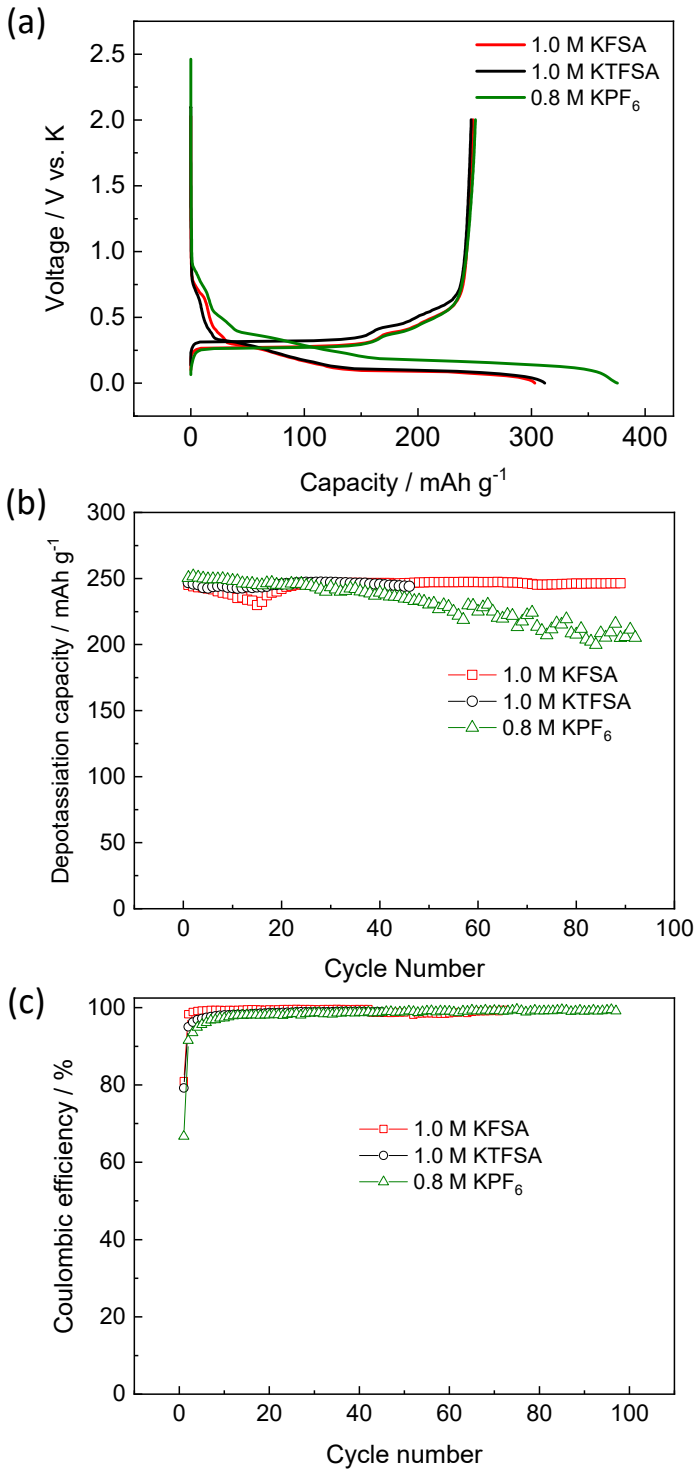

Figure S9 Electrolyte salt dependence. (a) Galvanostatic charge-discharge curves, (b) cycle stability, and (c) Coulombic efficiency of graphite electrodes with 5 wt% PANa binder in coin-type K cells tested in the voltage range of 0.0-2.0 V in the CC mode at 25 mA g^{-1}. 1.0 mol dm^{-3} KFSA/EC:DEC (= 1:1 v/v), 1.0 mol dm^{-3} KTFSA/EC:DEC (= 1:1 v/v), and 0.8 mol dm^{-3} KPF_6/EC:DEC (= 1:1 v/v) electrolytes were used.

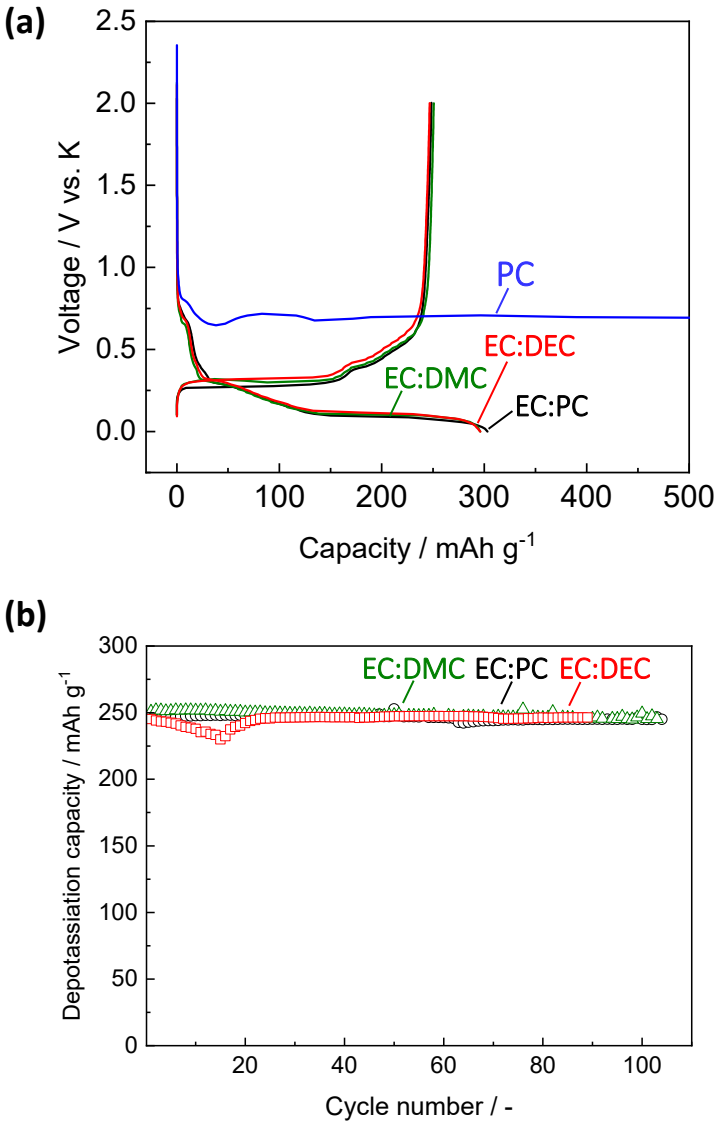

Figure S10 Electrolyte solvent dependence. (a) Galvanostatic charge-discharge curves and (b) depotassiation capacity of graphite electrodes with 5 wt% PANa binder in coin-type K cells tested in the voltage range of 0.0-2.0 V in the CC mode at 25 mA g^{-1}. Different solvent electrolytes of 1.0 mol dm^{-3} KFSA dissolved in EC:DMC (= 1:1 v/v), EC:DEC (= 1:1 v/v), EC:PC (= 1:1 v/v), and PC were used.

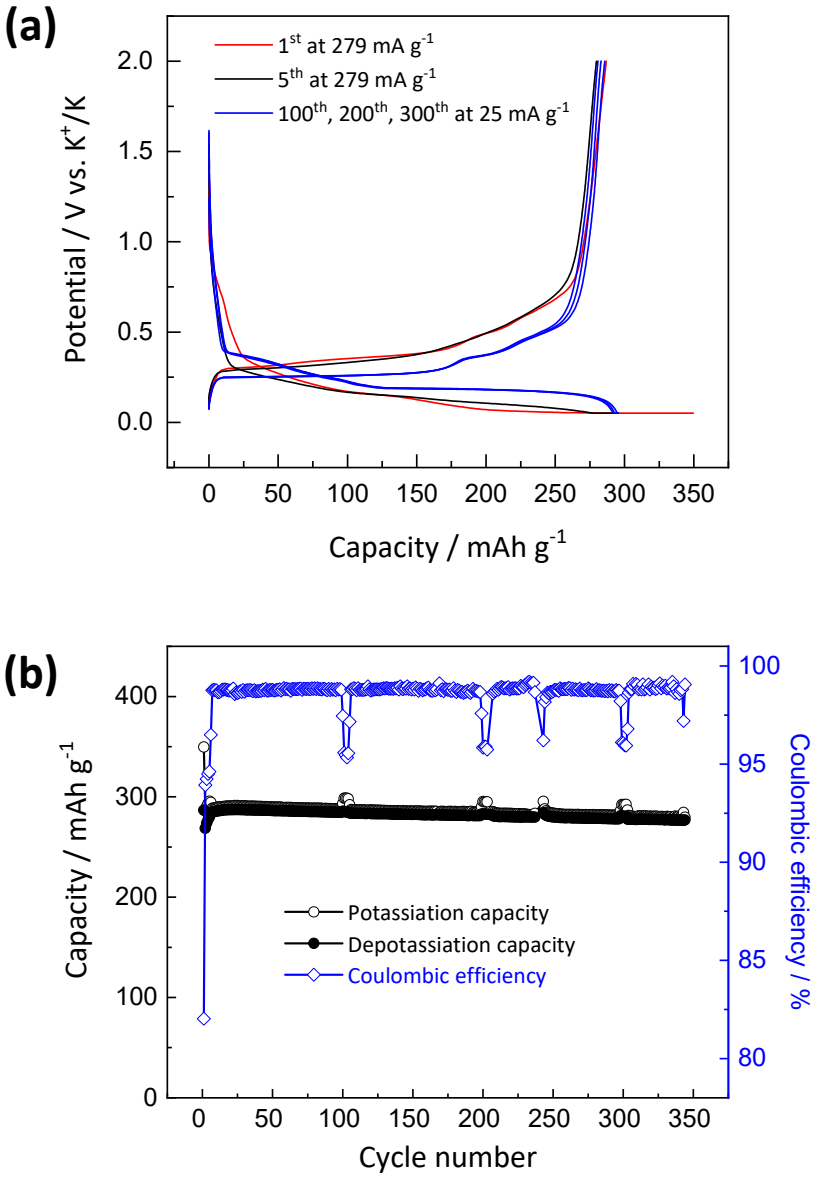

Figure S11 (a) Galvanostatic charge-discharge curves and (b) cycle stability and Coulombic efficiency of graphite electrodes consisting of 89 wt% SNO3, 6 wt% carbon black (TIMCAL super C45), and 5 wt% sodium carboxymethyl cellulose binder, tested in three-electrode type K cells and in the potential range of 0.002-2.0 V in the CC-CV mode at the current densities of 25 mA g^{-1} every 100 cycles and at 279 mA g^{-1} at the other cycles until reaching 0.002 V vs. K^+/K followed by potential keeping to 0.002 V vs. K^+/K for 5 h. 1.0 mol dm^{-3} KFSA dissolved in EC:DEC (= 1:1 v/v) was used. The dips in Coulombic efficiency are attributed to the slightly larger potassiation capacities than those of depotassiation. Slow rate potassiation/depotassiation processes every 100 cycles might induce partial dissolution of SEI into electrolyte or microcrack in the SEI film, resulting in the reformation of SEI on the subsequent potassiation process and the slightly lower Coulombic efficiency.

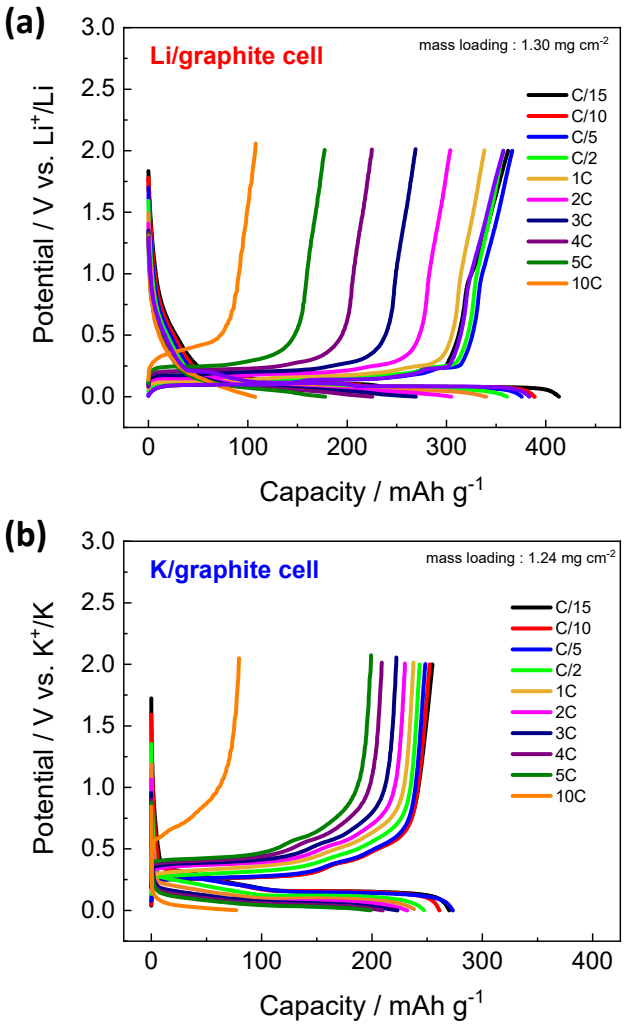

Figure S12 Discharge rate dependence. Galvanostatic charge-discharge curves of the three-electrode type (a) Li||graphite and (b) K||graphite cells charged (reduced) and discharged (oxidized) at the different current rates ranging from C/15-10C. 1.0 mol dm^{-3} AMFSA (AM = Li or K) /EC:DEC (= 1:1 v/v) electrolytes were used.

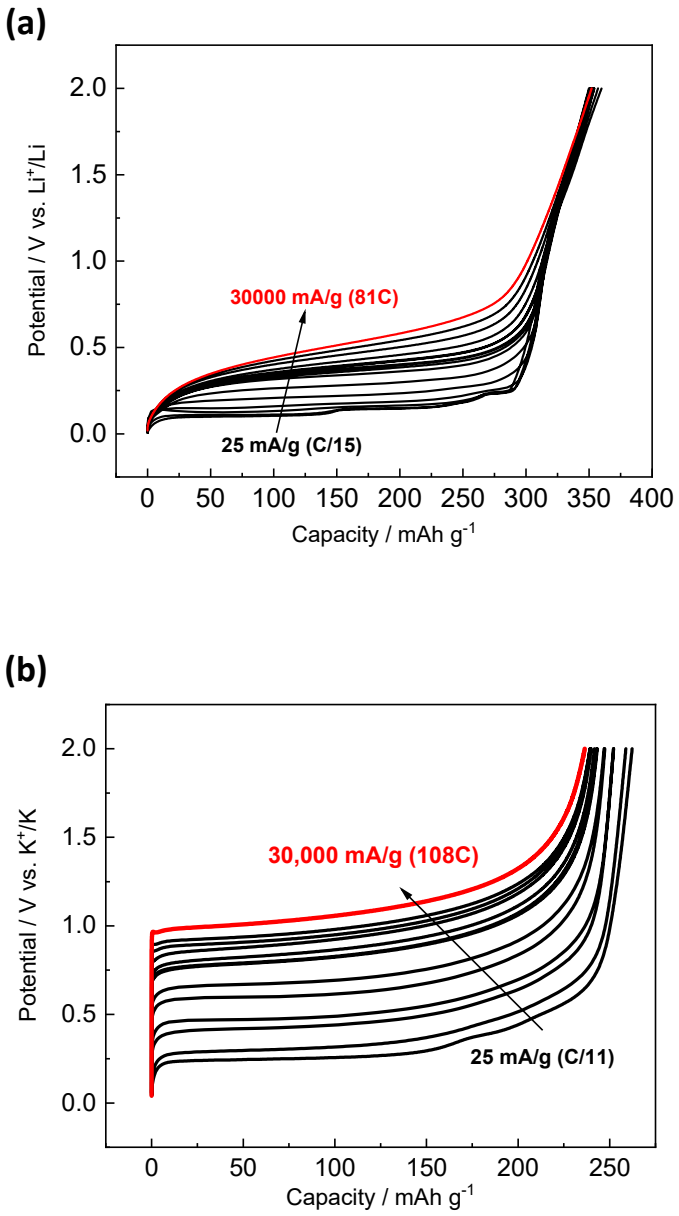

Figure S13 Charge-discharge rate dependence. Galvanostatic discharge curves of the three-electrode type (a) Li||graphite and (b) K||graphite cells tested at the different charging (reduction) and discharging (oxidation) current densities of 25-30,000 mA g^{-1}. 10 wt% PANa binder and 1.0 mol dm^{-3} AMFSA (AM = Li or K) /EC:DEC (= 1:1 v/v) electrolytes were used.

Table S1 Stacking sequence of graphene (A, B) and K (*α* (*β*'), *β, γ*, *δ*) layers of K_xC_8. The in-plane structures, including *α*, *β, γ*, *δ* positions are shown in Fig. 2. *β*' denotes the potassium sites between B type graphene layers.

Stage number	1	2	3	4
Stacking sequence	A*α*A*α*	AA*α*AA*α*	AAA*α*AAA*α*	ABAB*β*'BABA*α*
		AB*β*'BA*α*	ABA*α*ABA*α*	

Table S2 Predicted stable structures of K_xC_8, which can be described as $KC_{m\times n}$.

	x in K_xC_8	In-plane unit cell composition, KC_m	Stage number, *n*	Stacking sequence
KC_8	1	KC_8	1	A*α*A*β*A*γ*A*δ*
KC_{16}	1/2	KC_8	2	AA*α*AA*α*
KC_{24}	1/3	KC_8	3	ABA*α*ABA*α*
KC_{32}	1/4	KC_8	4	ABAB*β*'BABA*α*
KC_{56}	1/7	KC_{14}	4	ABAB*β*'BABA*α*

Table S3 Average interlayer distance d_{00n} for stage-*n* K-GICs.

Stage number *n*	Theoretical d_{00n} / Å (= (5.35 + 3.35(*n*-1))/*n*)	Theoretical d_{00n} / Å (DFT calculations)	Experimental d_{00n} / Å
1	5.350	5.343 5.526[a] 5.308[b]	5.345-5.354
2	4.350	4.374 (KC_{16}) 4.544 (KC_{16})[a] 4.360 (KC_{16})[b]	4.35-4.37
3	4.017	4.078 4.209[a]	4.01-4.08
4	3.850	3.923 (KC_{32}) 3.907 (KC_{56})	3.82-3.90
8	3.600	-	3.58-3.63

[a] Reference 1
[b] Reference 2

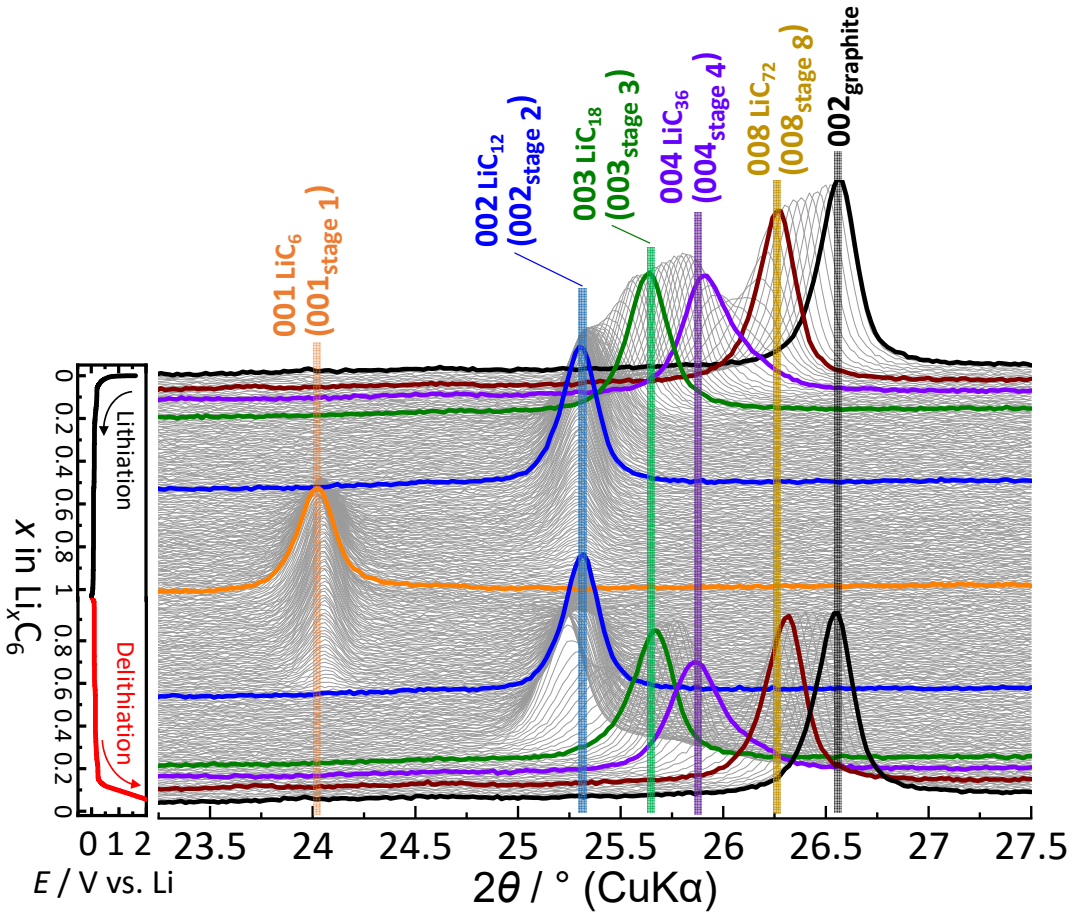

Figure S14 Enlarged *operando* XRD patterns of the graphite electrode with 10 wt% PANa binder in a two-electrode type Li cell.

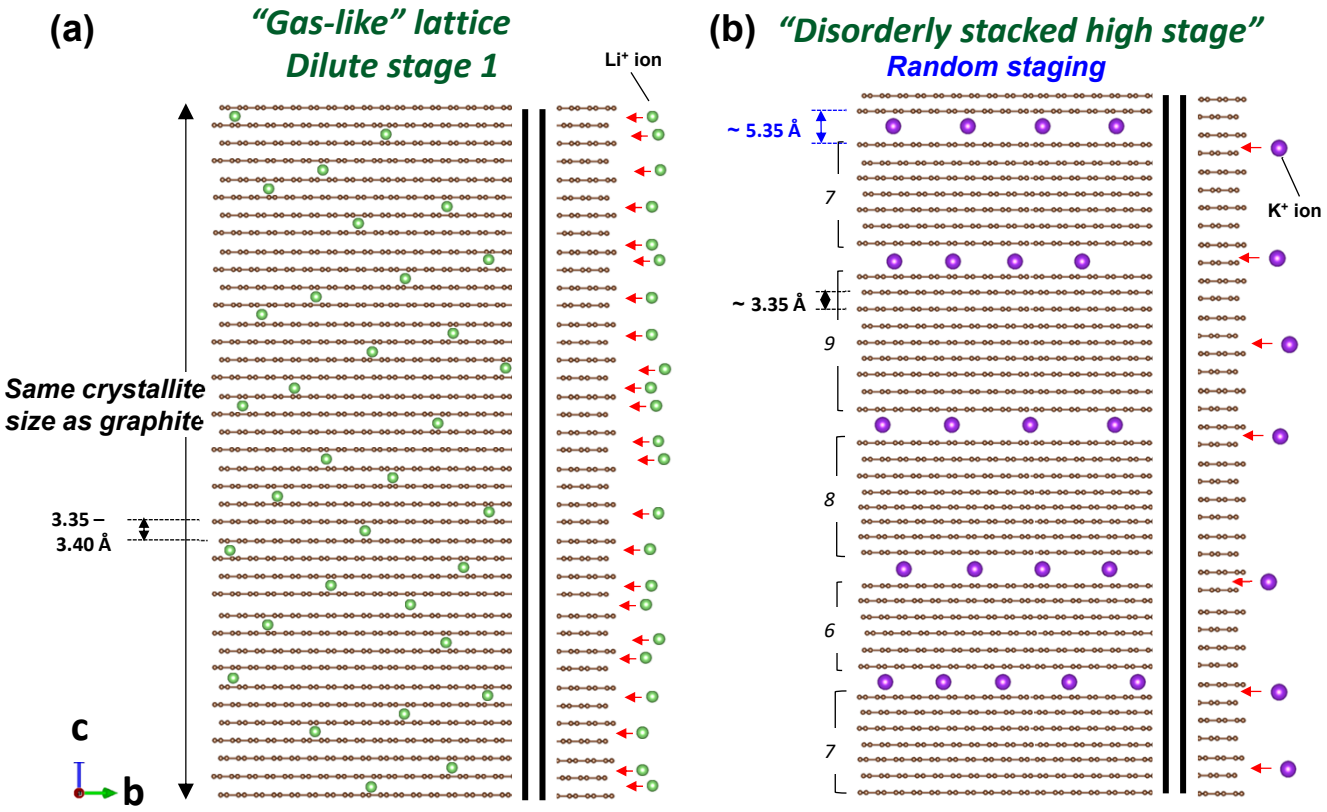

Figure S15 Schematic illustrations of initial staging processes for (a) dilute stage 1 Li-GIC and (b) disorderly stacked high stage K-GIC.

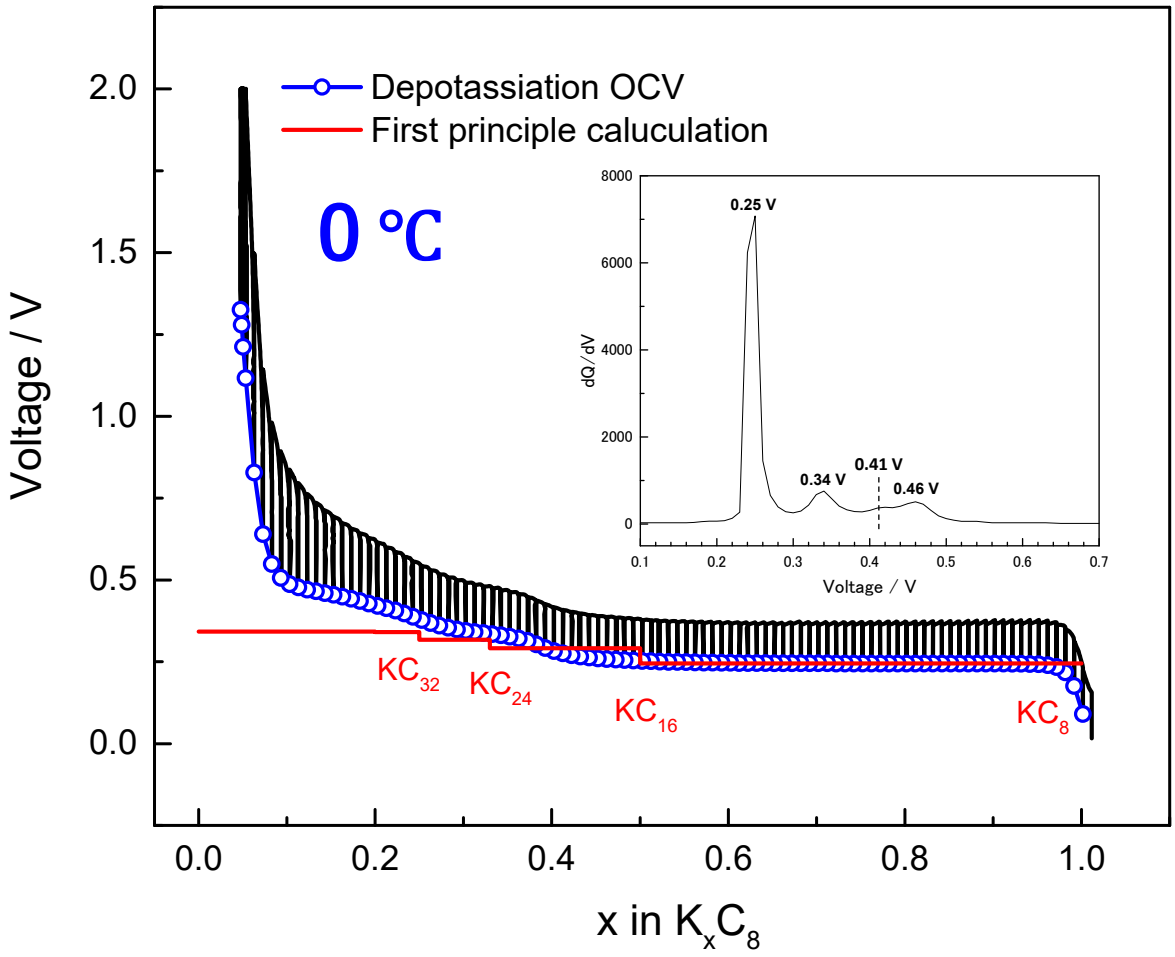

Figure S16 OCV profiles of the graphite electrode in a coin-type K cell. The cell was tested in the CC-CV mode at C/50 rate for 1 h followed by relaxation for 3 h at 0 °C after 5th galvanostatic charge cycle at 25 mA g^{-1} at 25 °C. 10 wt% PANa binder and 1.0 mol dm^{-3} KFSA/EC:PC (= 1:3 v/v) electrolyte were used. The d*Q*/d*V* curve of the OCV plots are shown in the inset.

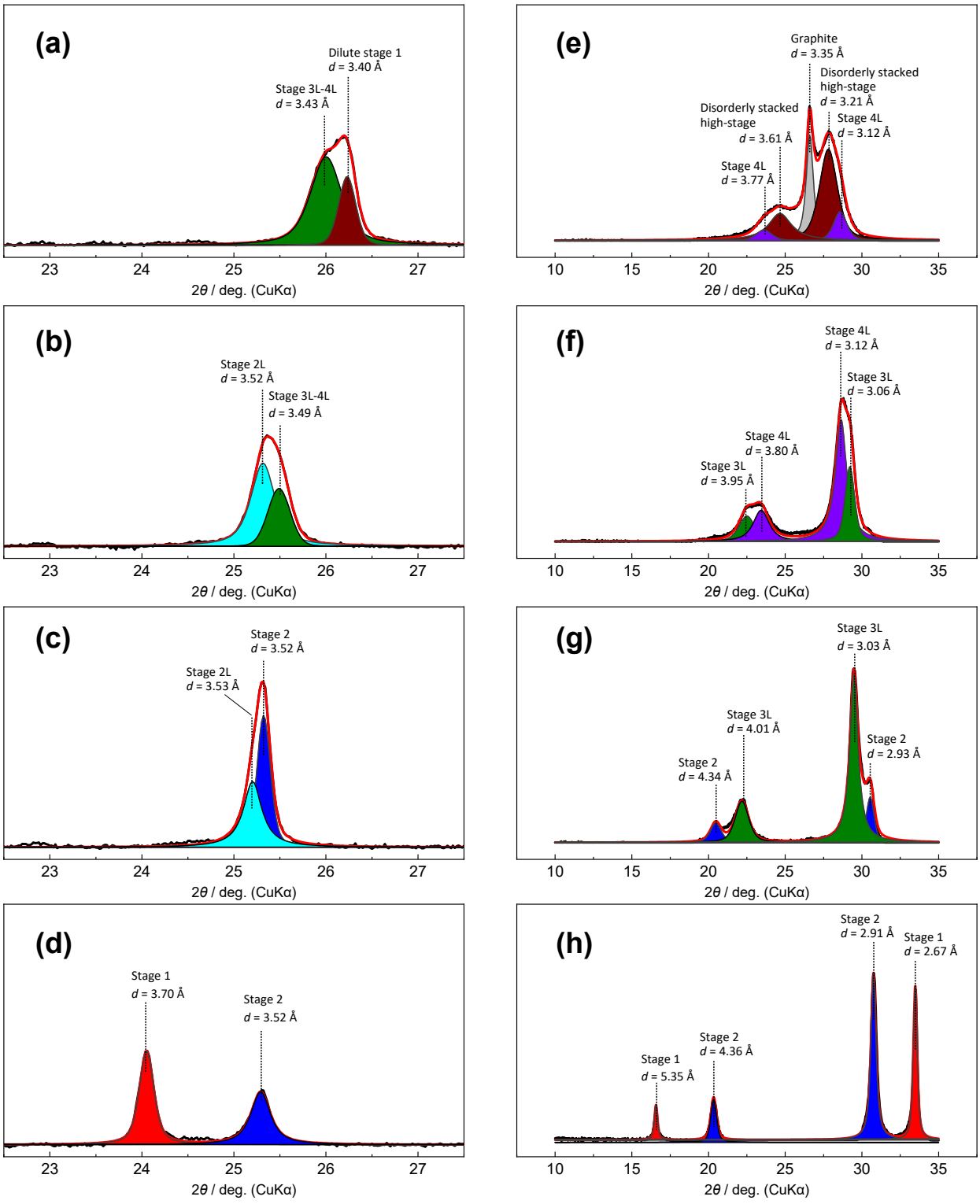

Figure S17 Selected *operando* XRD patterns for graphite electrodes: multiphases co-existence regions for (a) dilute stage 1 and stage 3L-4L, (b) stage 3L-4L and 2L, (c) stage 2L and 2, (d) stage 2 and 1 Li-GICs on a lithium deintercalation process, and (e) graphite, disorderly stacked high-stage, and stage 4L, (f) stage 4L and 3L, (g) stage 3L and 2 (2L), (h) stage 2 (2L) and 1 K-GICs on a potassium deintercalation process.

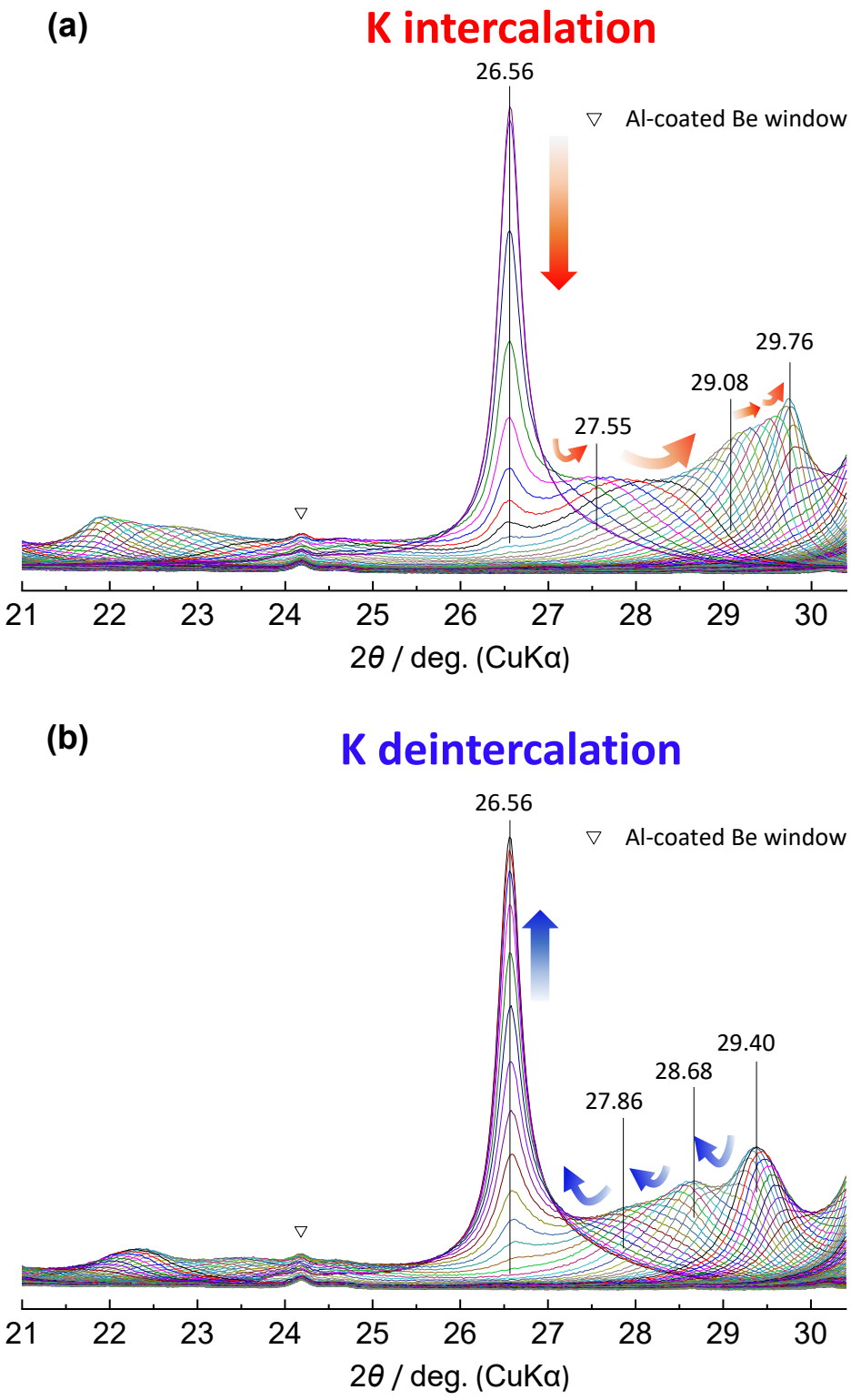

Figure S18 Selected operando XRD patterns without intensity offset for the graphite electrode in a two-electrode type K cell: (a) high stage and stage 4L-3L peaks during K intercalation process and (b) stage 3L and 4L and high-stage peaks during K deintercalation process.

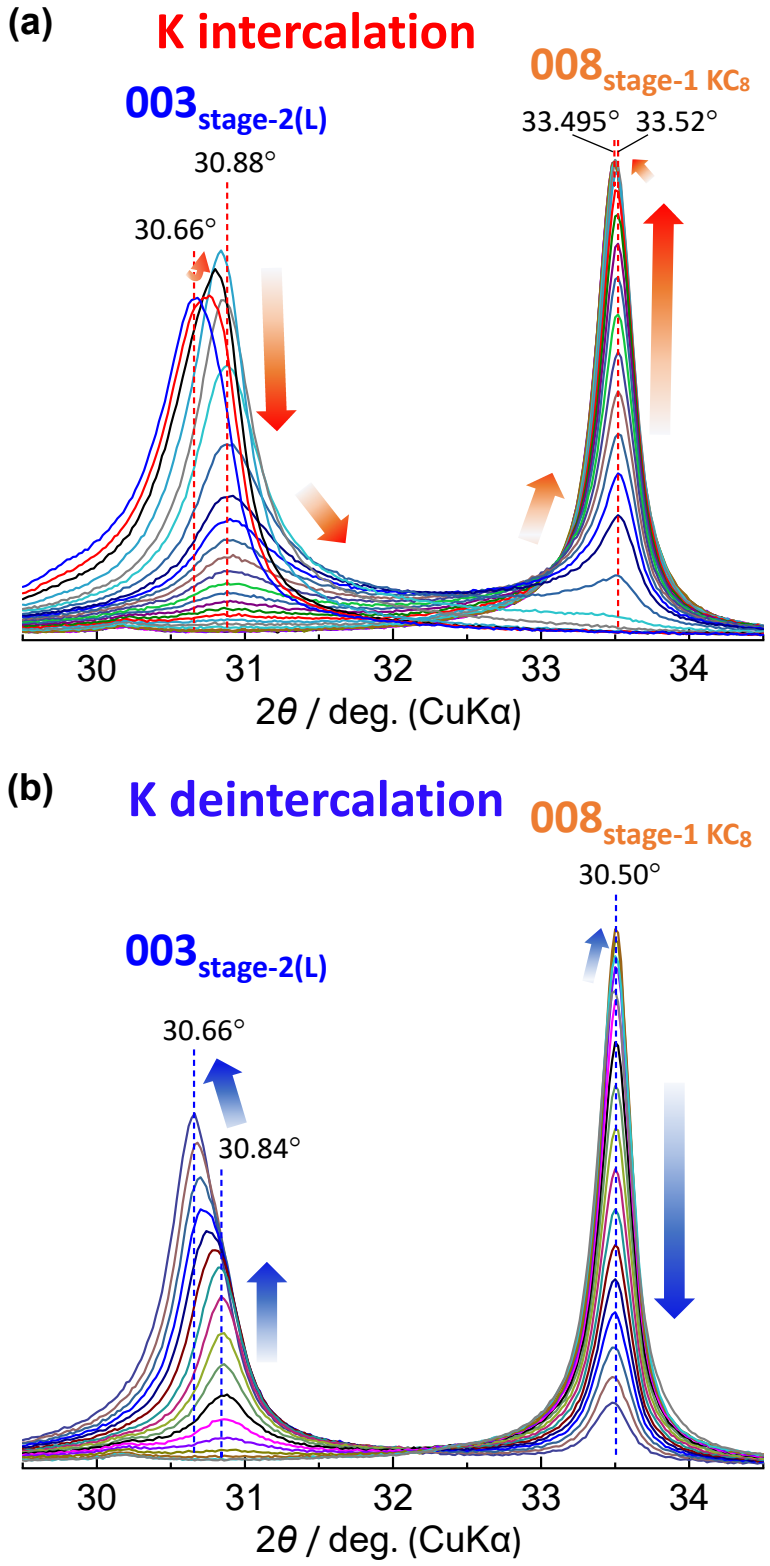

Figure S19 Selected *operando* XRD patterns without intensity offset for the graphite electrode in a two-electrode type K cell: stage 1 and 2(L) peaks corresponding to 00*n*+1 reflections during (a) K intercalation and (b) K deintercalation processes.

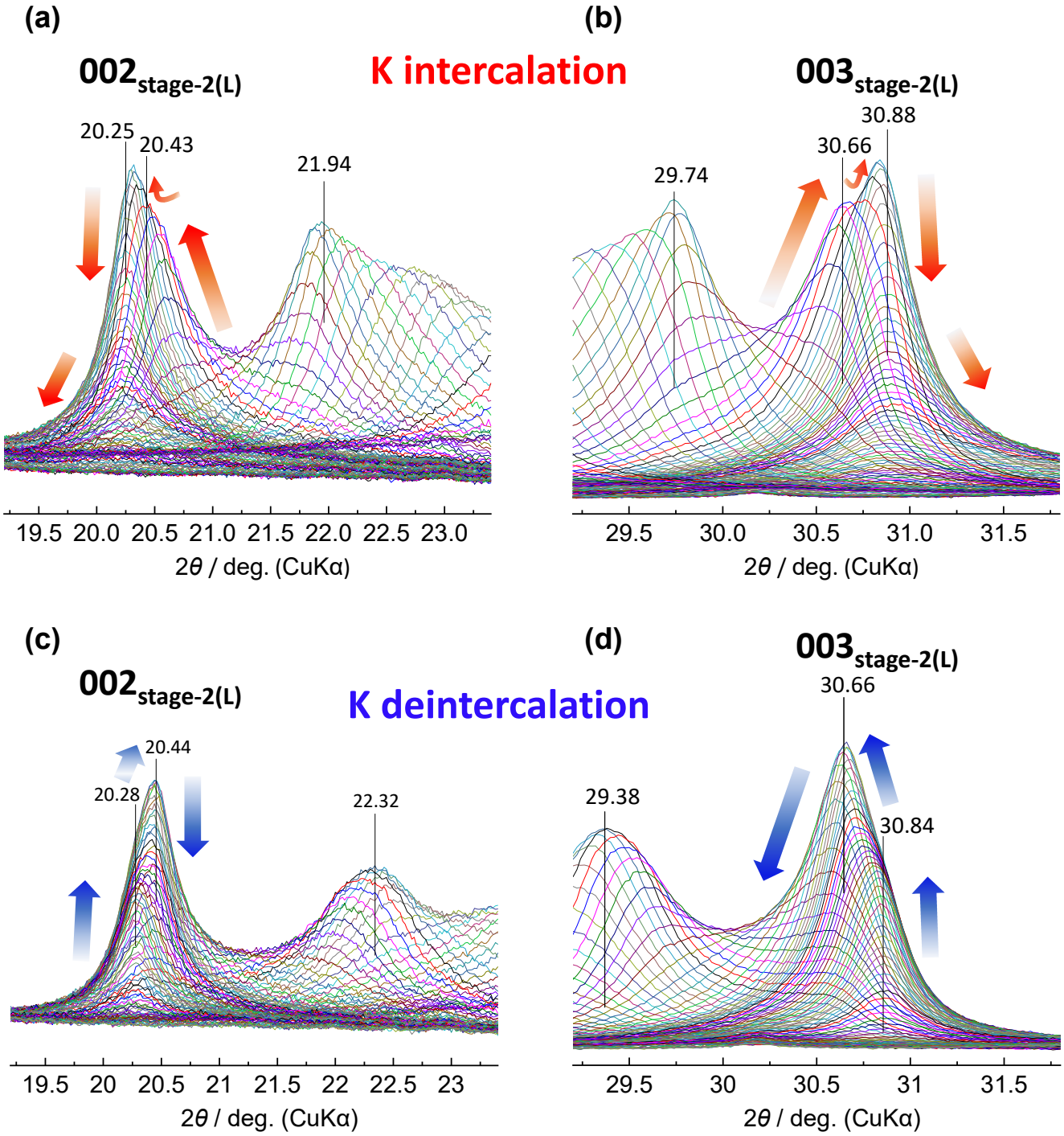

Figure S20 Selected *operando* XRD patterns without intensity offset for the graphite electrode in a two-electrode type K cell: stage 2L/2 peaks at the (a, c) low angle (b, d) high angle regions during (a, b) K intercalation and (c, d) K deintercalation processes.

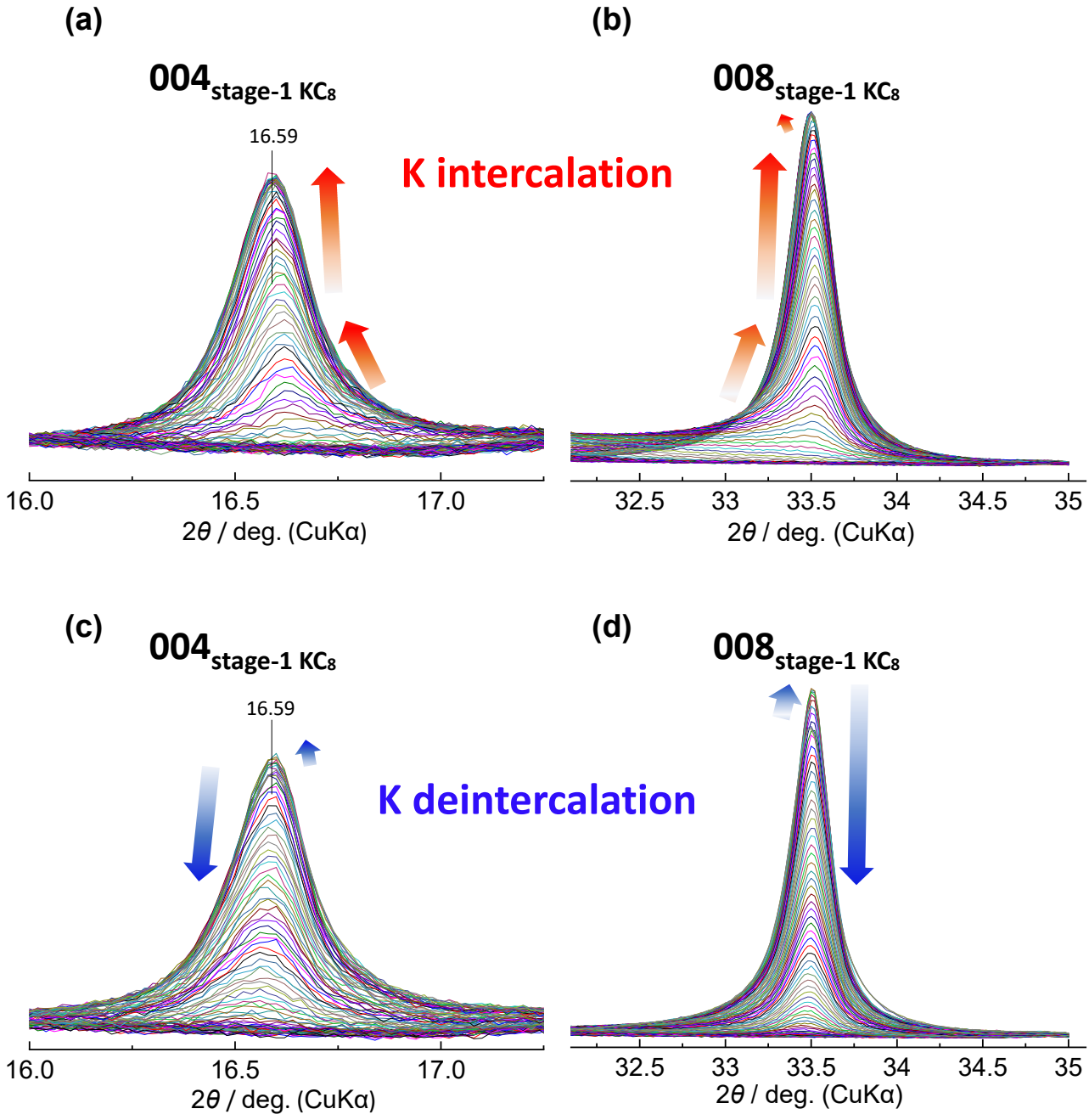

Figure S21 Selected *operando* XRD patterns without intensity offset for the graphite electrode in a two-electrode type K cell: stage 1 peaks at the (a, c) low angle (b, d) high angle regions during (a, b) K intercalation and (c, d) K deintercalation processes.

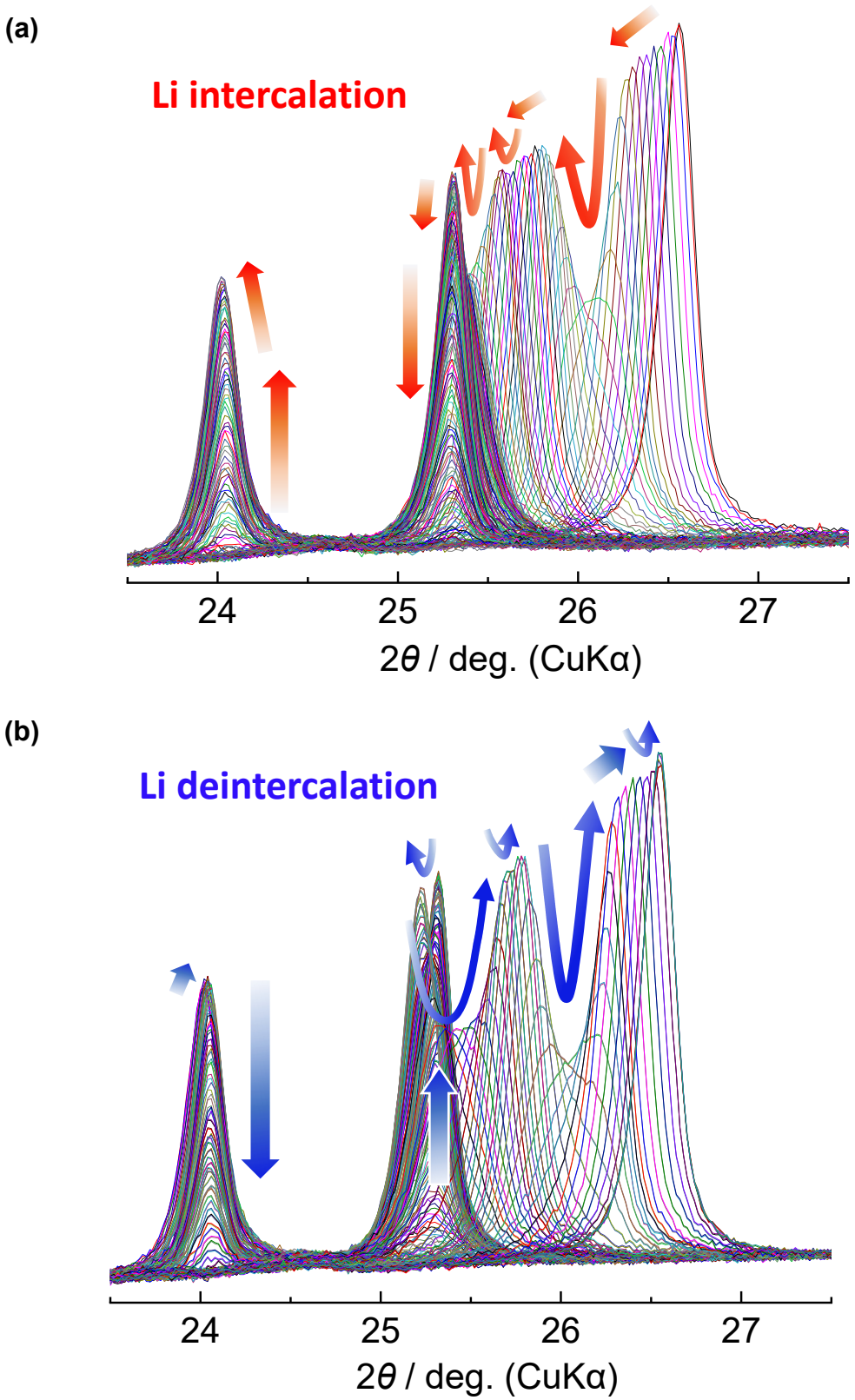

Figure S22 O*perando* XRD patterns without intensity offset for the graphite electrode in a two-electrode type Li cell during (a) Li intercalation and (b) Li deintercalation processes.

References

1. W. Luo, J. Wan, B. Ozdemir, W. Bao, Y. Chen, J. Dai, H. Lin, Y. Xu, F. Gu, V. Barone and L. Hu, *Nano Lett.*, 2015, **15**, 7671-7677.
2. O. Lenchuk, P. Adelhelm and D. Mollenhauer, *Phys. Chem. Chem. Phys.*, 2019, **21**, 19378-19390.